4.5.2 Test materials (by B.G.Gireń and J.Steller)

General remarks

Significant differentiation of material performance under different cavitation conditions cannot be explained without physical interpretation of the phenomena induced in the surface layer. The material erosion development is closely linked to plastic deformations and fatigue processes occurrence. Pronounced processes deflect the state of the *solidi* from the equilibrium more and more until its loses its stability. Further decomposition of the material is approximately proportional to the amount of the energy delivered by cavitation impacts of specified class to the surface layer. The above statement is more exact, the more uniform internal state the eroded layer is and the less interaction with the bulk material takes place.

The volume loss curves resulting out of predominant plastic deformation effect are usually featured by a relatively short incubation period needed to deform the surface geometry in a way enabling efficient removal of the material by subsequent pressure waves and liquid microjets. The initial stage of fatigue erosion is characterised by internal deformations including grain slips and twinning as well as formation of deformation bands and Luders lines. Slip occurs in the *bcc* lattice (e.g. in ferritic steels) by glide of dislocations with Burgers vector of type *a/2* <111> on {110}, {211} and {321} planes. Deformation by mechanical twinning is more restricted and is thought to occur by movement on {211} planes of partial dislocations with Burgers vector of type *a/6* <111>. In the *fcc* lattice (e.g. in austenitic steels) slip occurs by movement of dislocations with Burgers vector of type *a/2* <110> on {111} planes. In this lattice deformation by twinning is not common [20].

In brittle materials mass movement is confined and accumulation of stresses occurs more readily, which contributes to inception of cracks at the weak points and their subsequent intergrain or intragrain propagation. In ductile materials dislocations generated under the cavitation loading are put in motion and eventually stanched, being blocked mutually or by precipitations. In the first case the heaped up dislocations creates the new substructure of the grains, whereas in the latter case they result basically in such structural changes like the changes of grains size, positioning and/or geometry. The processes mentioned may lead to the work hardening effect. This is especially the case for alloys steels featured by a metastable austenitic structure.

In numerous practical applications corrosion/erosion interference is inevitable. As it has been shown in section 4.3 of this report, such a phenomenon had a major effect on test results in the cavitation tunnel of the Hiroshima University. Including corrosion processes in the general analysis of the cavitation erosion progress is a very difficult task and will not be attempted here.

In the next subsections a brief description of erosion progress and changes taking place in the test material structure will be given following the much more detailed analysis accomplished in [21]. The metallographic analysis is based on the photographic documentation submitted by the TSING, HULL and CAP labs.

PA2 aluminium alloy

This material is known to be characterised by extremely low hardness and ultimate strain values (Table 4). The damage produced by plastic deformation of the surface layer (Fig.8,9) was usually much higher than that of other materials. The only exceptions include:

- Tsinghua vibratory rig where tarnamide plastics eroded much faster than all other materials,
- CSSRC rotating disk and HAN cavitation tunnel where PA2 has shown longer incubation period than the M63 brass.

It should be noticed that in both cases mentioned the maximum and ultimate values of the PA2 erosion rate are several times higher than those of the M63 brass.

M63 brass

As it can be seen from Table 4, also the M63 brass is characterised by low hardness (about 2.3 times lower than that of the 45 and 1H18N9T steels) and low tensile strength. Its yield point is even lower than that of the PA2 aluminium alloy.

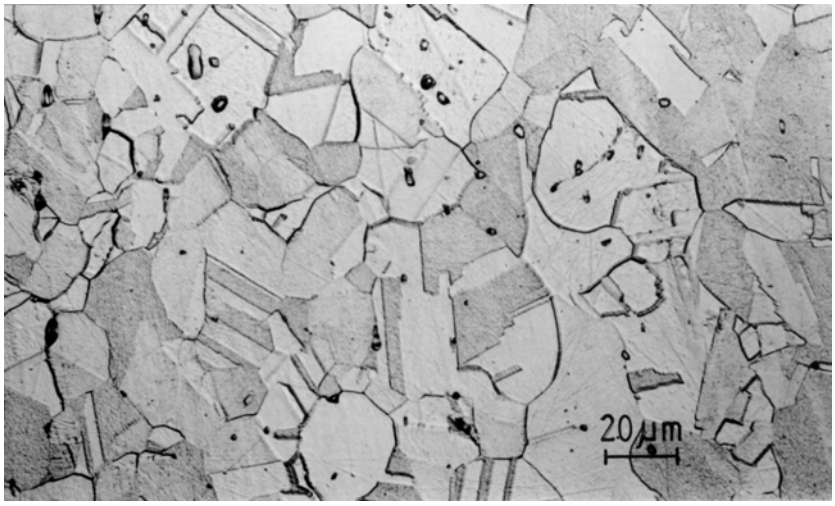

Fig.33 Optical microscopy of the M63 brass structure (University of Cape Town lab)

The optical microscopy of the bulk material taken at the University of Cape Town (Fig.33) reveals a structure consisting of α *phase* mottled grains, some of them equiaxied and of high energy at interconnections. Numerous non-metallic precipitations are visible. At metallographs of the University of Hull and the Tsinghua University of Beijing (cf. Part II of the report) areas of depleted matrix with possible structure of $\beta + \alpha$ (β phase: CuZn, *bcc* structure) can be detected.

Very developed line of damaged edge of the sample is presented in Figure 11. Plastic deformations due to slip bands, planar and wavy slips, deformation bands can be detected. Cracks nearby the surface are of ductile nature. The local concentrations of deformation under the surface are visible, maybe due to intersecting of the slips or stress concentration around the precipitation. The cracks detected in the surface layer at higher magnification (Fig.34) seem to be transcrystallic. Fragments of the material extracted from the surface are also visible. Final grain shape is quite variable and reflects an unusual degree of nonuniformity of plastic strain from grain to grain.

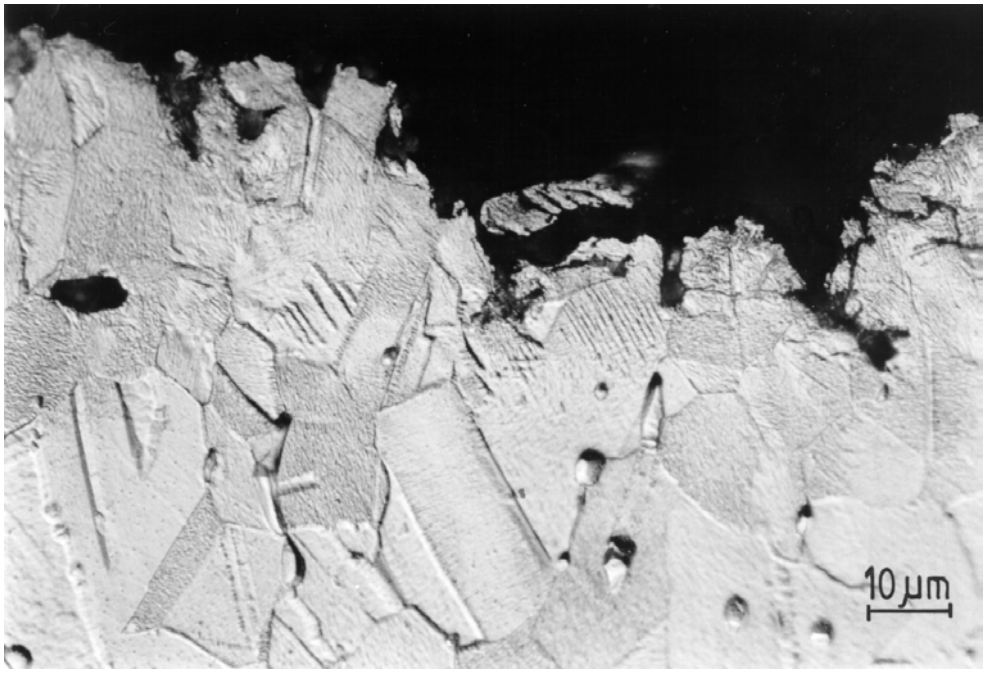

Fig.34 High magnification of the M63 brass structure beneath the cavitated surface (University of Cape Town lab)

Erosion curves of the M63 brass lie usually well below the PA2 aluminium ones and above those of the E04 Armco iron. However, at vibrating specimen vibratory rigs characterised by high cavitation intensity (CISE, IMP), the M63 brass performs even better than the E04 iron. This can be due to the work hardening effect which was stated beyond any doubts in the CAP and HULL labs (hardness increase of 30 ÷ 40 %). No such effect took place in the TSING lab where the intensity of cavitation was substantially lower.

In one case (CSSRC rotating disk) the M63 performed better than the 45 carbon steel which evokes questions whether the proper material was tested.

E04 Armco iron

The material is featured by hardness about 30 % higher than that of the M63 brass, almost the same tensile strength and twice higher yield point value. Both the hardness and tensile strength are twice smaller than those of the 45 and 1H18N9T steels.

The ferritic grains of different size and directional positioning can be seen from the metallograph in Fig.35a. A few non-metallic precipitations can be also detected in the photograph. The lack of noticeable plastic deformations at the cavitated edge of the sample is the main feature of the structure presented in Fig.35b. The plastic deformations in the surface layer are not very extensive. It is not surprising as the plastic deformations in the materials of centred regular lattice consist in brittle cracks and twinning. The deformation twins, however, can be found only in the photographs received from the Tsinghua University although no increase of their number in effect of cavitation loading can be stated here. The transcrystallic cracks leading to grains dividing and subsequent removal of the material pieces nearby the surface can be inferred from Fig.35c. in structural singularities.

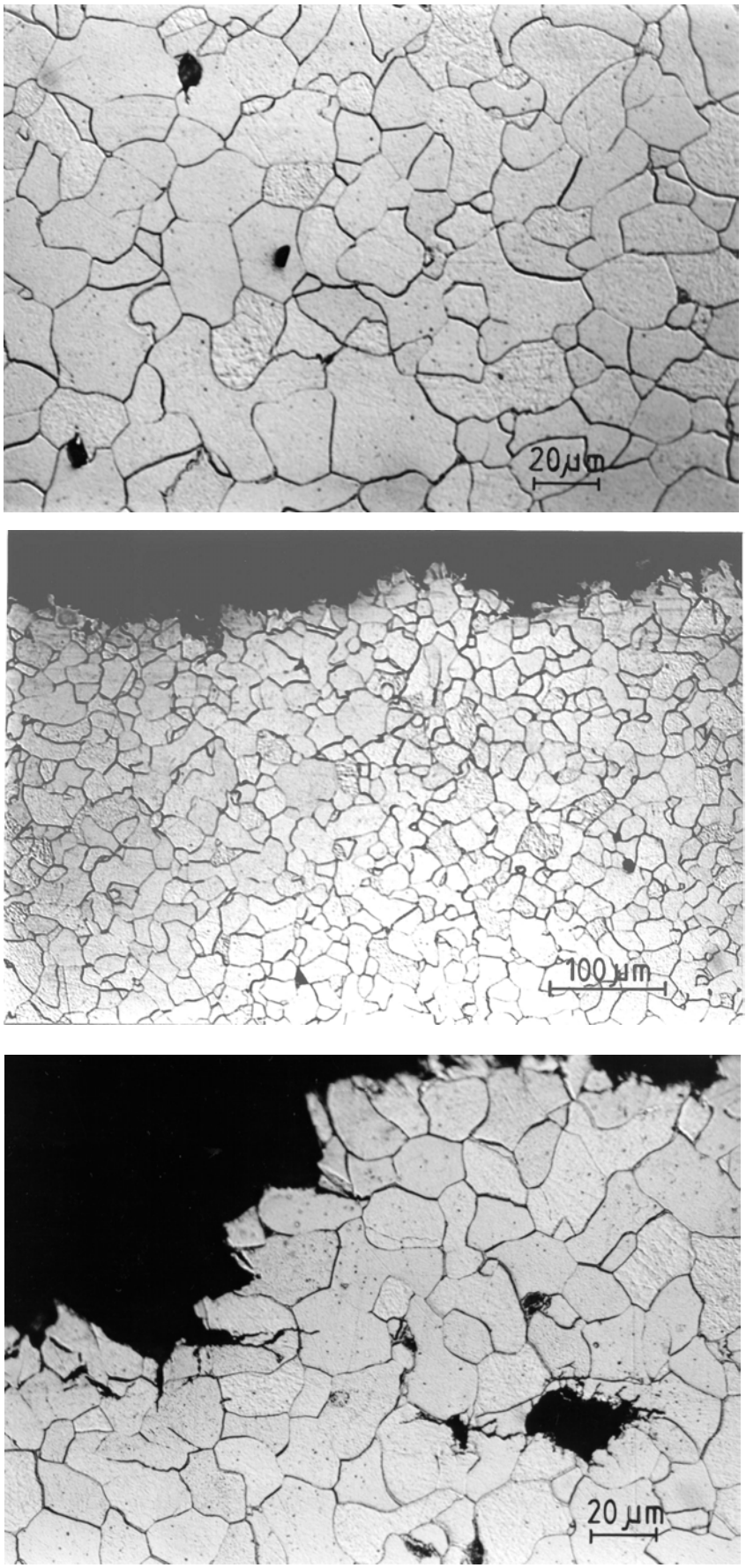

Fig.35 Optical microscopy of a cross section of an Armco iron specimen: a) microstructure in the centre of the specimen, b,c) cavitated edge (University of Cape Town lab)

Attention should be paid to the very large amount of cracks in the material surrounding the non-metallic precipitations.

The revealed sub-grains structures as well as the dislocation bands within the grains of ferrite indicate transfer of huge stresses through the surface layers and their accumulation. Armco iron was included in the Test Programme as the basic reference material. Its performance was usually slightly worse than that of the M63 brass. Very high difference of erosion rates was stated during tests conducted in the cavitation tunnel of the City University and one series of tests in the cavitation tunnel of the University of Hannover. In cases mentioned above an inversion of the M63/E04 ordering has been stated.

In Tsinghua University the volume loss of Armco iron has been even smaller than that of the 45 carbon steel. The erosion curves of both materials tested at the liquid jet facility in the SIGMA V.U. are almost the same. In both cases a question can be put whether the proper material was tested. The similar relationship results from the tests conducted using the Lichtarowicz cell at the University of Hannover. In this case, however, the incubation period for the 45 steel is several times higher than that for the E04 Armco iron.

45 carbon steel

This material is characterised by the highest tensile strength and yield point value of all the metallic materials tested. However, the ultimate strain exceeds only by 30 % that of the PA2 aluminium alloy.

Microstructure in the centre of the specimen shown in Fig.36a consists of ferrite and pearlite (ferrite$_P$ + Fe_3C) and to some extent bainite (α phase oversatured with carbon and cementite of a specific needle-like shape) grains. The strips of carbide precipitation are visible. The cavitated edge is quite smooth - the whole surface subjected to the erosion is destroyed uniformly (Fig.36b). An observation of the edge line structure in Fig.36c leads to the conclusion that ferritic grains are removed first as a weaker component of the structure. The cracks and pits near the surface appear and develop mainly in the interior of ferrite grains. The pieces of pearlite or bainite are subsequently extracted as a result of splits and cleavages.

The 45 carbon steel was almost always the second most resistant metallic material tested although the ratio of erosion rates between this material and the 1H18N9T steel varied in a rather wide range. In some rigs of high cavitation intensity (CISE vibratory rig, PEITZ cavitation tunnel) the performance of this material was even better than that of the 1H18N9T steel. In two cases of high intensity rigs (CAP vibratory rig and IMP rotating disk) the performance of both materials was practically the same. The peculiarities include:

- the TSING vibratory rig where the performance of the 45 steel specimens was worse than that of the E04 Armco iron (cf. subsection above),
- the SIGMA liquid jet facility where the Armco iron and 45 carbon steel curves almost coincide (cf. subsection above),
- the CSSRC rotating disk where the 45 steel performed worse than the M63 brass,
- the HIRO cavitation tunnel where complete re-ordering of results has taken place,
- the Lichtarowicz cell in Hannover where the maximum and ultimate volume loss rate of this material was higher than that of the E04 Armco iron despite much longer incubation period.

Tests conducted at flow test rigs and the cavitating jet cells prove substantial incubation periods which suggests the 45 steel fatigue as the main erosion mechanism.

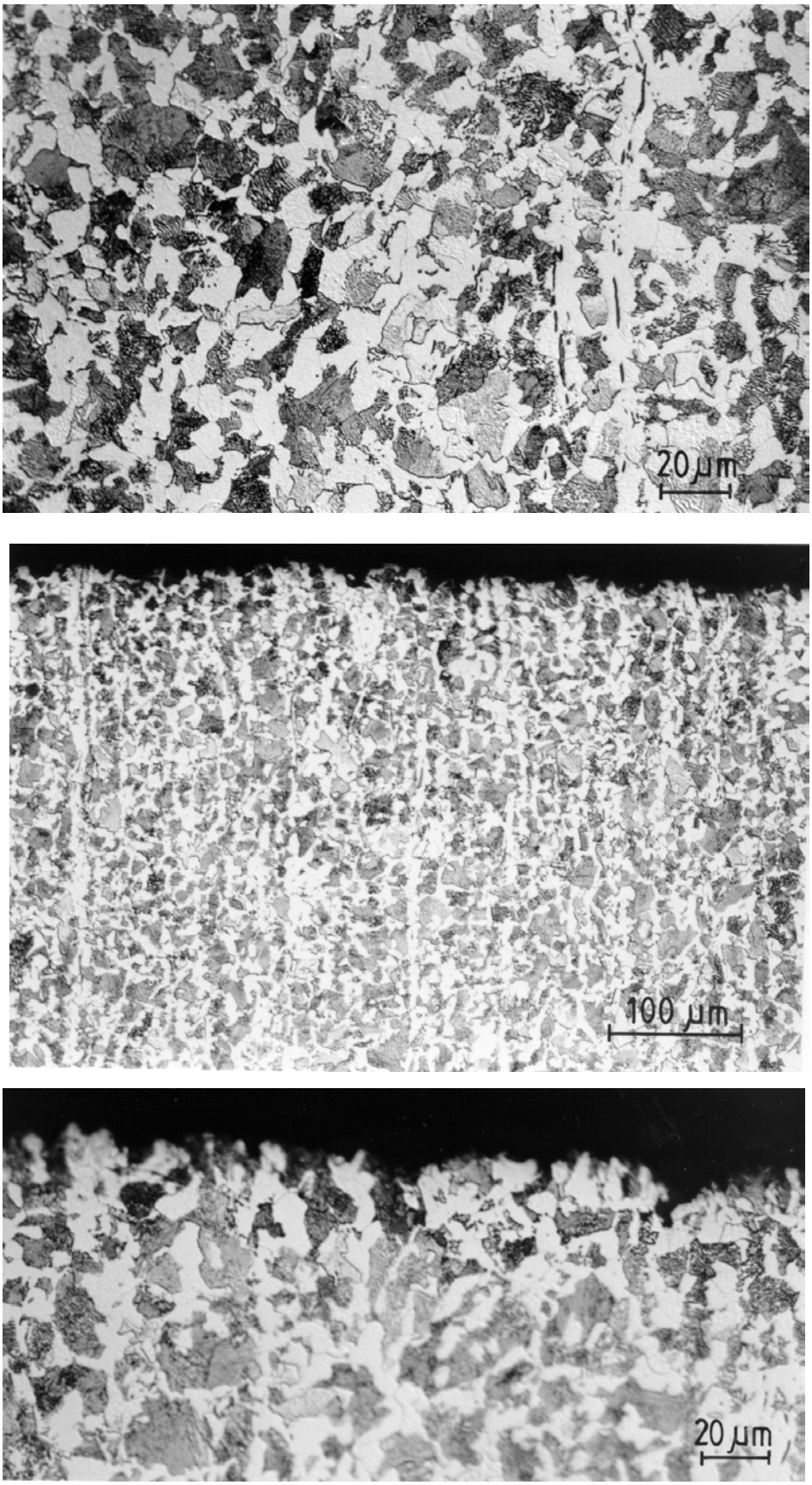

Fig.36 Optical microscopy of a cross section of a 45 carbon steel specimen: a) microstructure in the centre of the specimen, b,c) cavitated edge (University of Cape Town lab)

1H18N9T chromium-nickel steel

This is austenitic “self-hardening” steel characterised by the yield point almost twice smaller and the ultimate strain over twice higher than that of the 45 carbon steel.

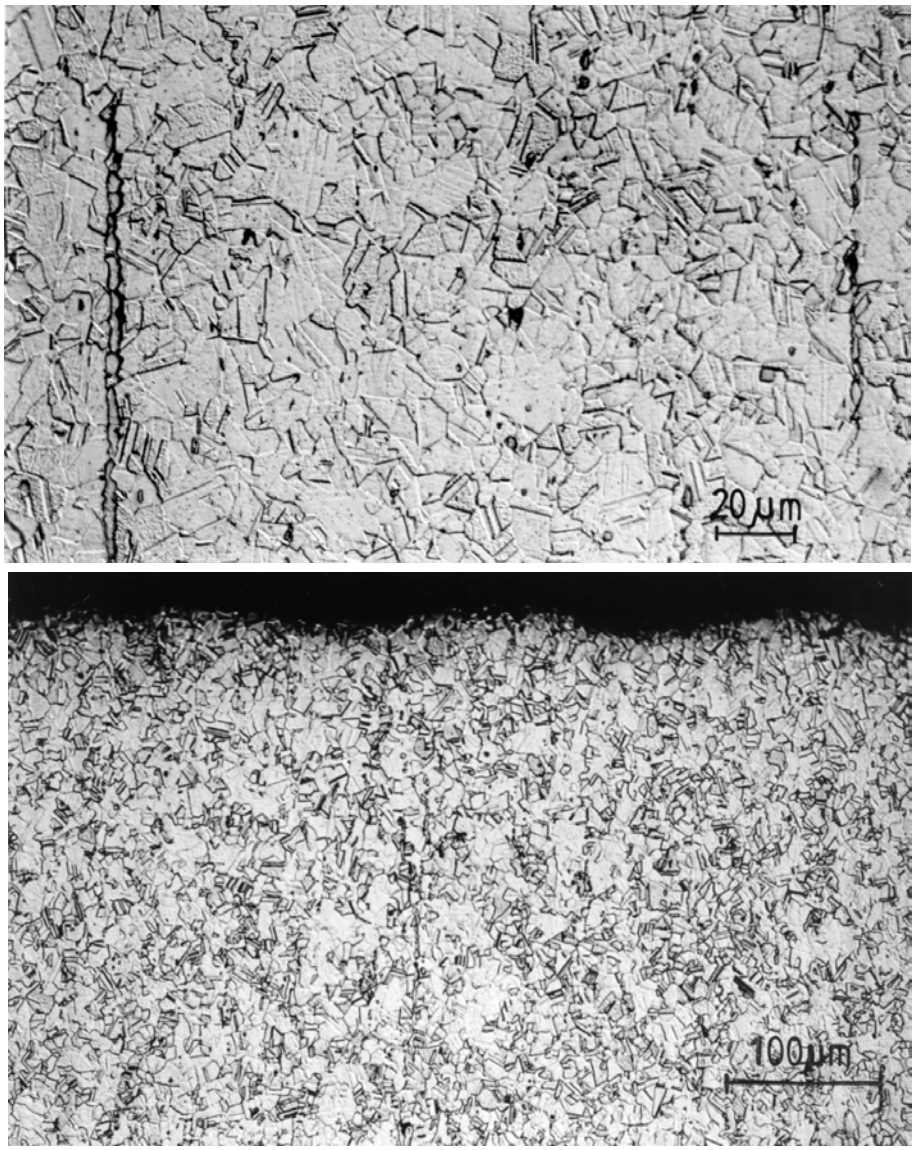

Fig.37 Optical microscopy of the microstructure in the centre and at the edge of the 1H18N9T steel specimen in the University of Cape Town lab

The microstructure shown in Fig.37a seems to be austenite with large amount of recrystalization twins. The dimensions of the grains are very small. Some darker grains should be recognised as ferrite (Fig.37b). There are also very small point precipitations of carbides. A destroyed surface with splits and cleavages is shown in Fig.38. Apart from splits, the ductile cracks seem to play some role in the process of material destruction. The deformation bands as well as the shear bands are clearly visible in the interior of some grains. The structure is very compact which gives rise to the transcrystallic cracks development.

Generally, the 1H18N9T has performed much better than all other metallic test materials. This is surely due to substantial work-hardening which resulted sometimes (University of Cape Town) in a 40 % increase of hardness. In few cases (CISE and CAP vibratory rigs, IMP rotating disk, PEITZ cavitation tunnel) the performance of the 1H18N9T steel was the same

as or slightly worse than that of the 45 carbon steel. It is noticeable that this inversion is confined to rigs of very high cavitation intensity. A complete exception is the HIRO cavitation tunnel where the only material eroding faster then the 1H18N9T steel is the PA2 aluminium alloy (cf. previous subsections).

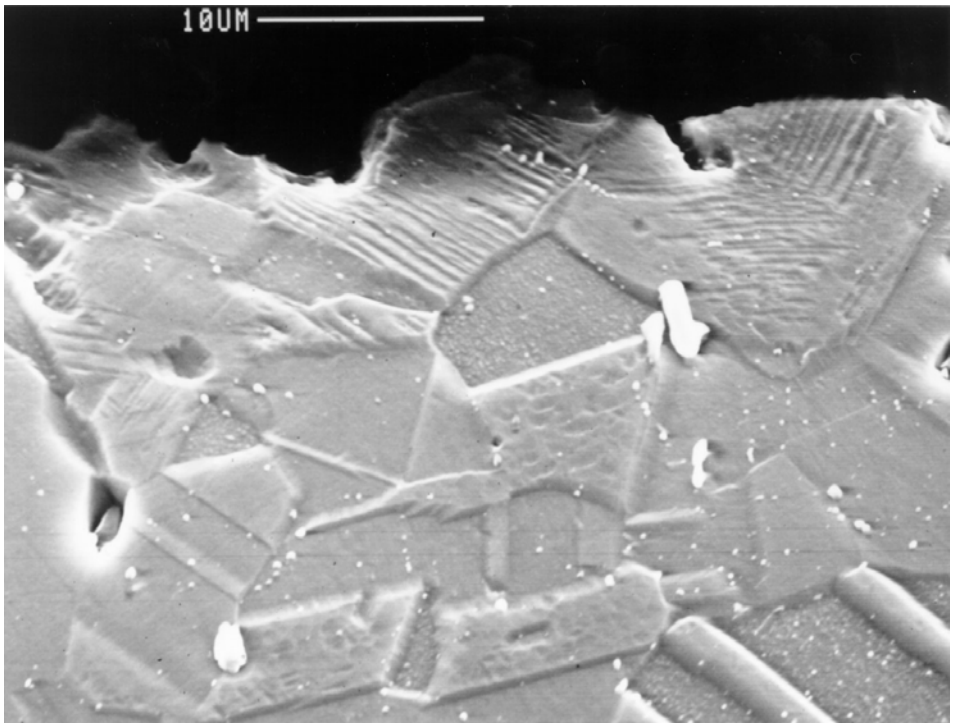

Fig.38 Scanning electron microscopy of the cavitated edge of a 1H18N9T specimen (University of Cape Town lab)

polyamide 6 plastics (tarnamide)

As already mentioned in section 3, it was only in the IMP PAN, at the Tsinghua University and at the University of Cape Town where vibratory tests allowed to plot the cumulative mass/volume loss curves for the tarnamide plastics. In the last case the mass loss curve was determined after applying special technique with a reference specimen. The only lab having determined the erosion curve at a cavitation tunnel is the Pumped Storage Power Plant Hohenwarte II (VK-AG Peitz). As already mentioned, tests at rotating disks and the liquid impact device have appeared more successful which seems due to substantial amount of powerful pressure pulses.

As it can be seen from photographs submitted by Prof. A.Ball of the University of Cape Town, tarnamide erosion developed here by spreading of brittle cracks in the bulk of material tested (Fig.39). It is clear that such an erosion mechanism could promote efficient absorption of liquid. Brittle erosion mechanism at the rotating disk in IMP PAN is indicated by the erosion curves in Figs 21 and 32.

Comparison of tarnamide performance with that of other materials brings ambiguous results. Using the mass loss related criteria one can state that tarnamide performed usually better than the 1H18N9T steel. However in case of intense cavitation, characterised by significant fraction of high amplitude pulses (PEITZ cavitation tunnel, SIGMA liquid jet device) the material can perform worse than the M63 brass. Interpretation of the TSING results (extremely high erosion rate) is difficult and may rise essential doubts due to very short test duration.

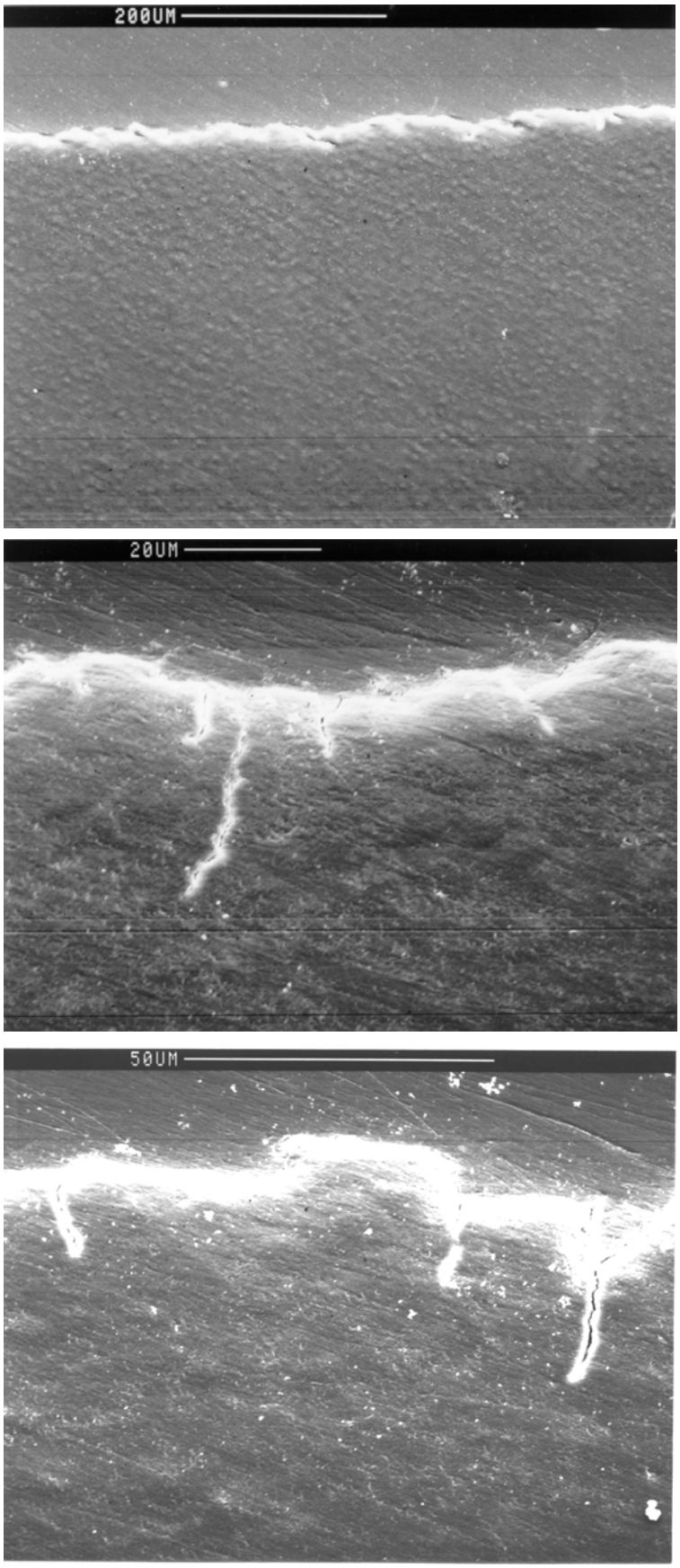

Fig.39 Scanning electron microscopy of a tarnamide specimen cross-section (University of Cape Town lab)